J Membrane Biol (2013) 246:633–645
DOI 10.1007/s00232-013-9577-0

Role of Outer-pore Residue Y380 in U-type Inactivation of $K_V2.1$ Channels

Quentin Jamieson · Stephen W. Jones

Received: 26 February 2013 / Accepted: 10 June 2013 / Published online: 28 June 2013

Abstract The interpretation of slow inactivation in potassium channels has been strongly influenced by work on C-type inactivation in *Shaker* channels. Slow inactivation in *Shaker* and some other potassium channels can be dramatically modulated by the state of the pore, including mutations at outer pore residue T449, which altered inactivation kinetics up to 100-fold. $K_V2.1$, another voltage-dependent potassium channel, exhibits a biophysically distinct inactivation mechanism with a U-shaped voltage-dependence and preferential closed-state inactivation, termed U-type inactivation. However, it remains to be demonstrated whether U-type and C-type inactivation have different molecular mechanisms. This study examines mutations at Y380 (homologous to *Shaker* T449) to investigate whether C-type and U-type inactivation have distinct molecular mechanisms, and whether C-type inactivation can occur at all in $K_V2.1$. Y380 mutants do not introduce C-type inactivation into $K_V2.1$ and have little effect on U-type inactivation of $K_V2.1$. Interestingly, two of the mutants tested exhibit twofold faster recovery from inactivation compared to wild-type channels. The observation that mutations have little effect suggests $K_V2.1$ lacks C-type inactivation as it exists in *Shaker* and that C-type and U-type inactivation have different molecular mechanisms. Kinetic modeling predicts that all mutants inactivate preferentially, but not exclusively, from partially activated closed states. Therefore, $K_V2.1$ exhibits a single U-type inactivation process including some inactivation from open as well as closed states.

Keywords U-type inactivation · Voltage-gated potassium channels · Kinetic models · Outer pore

Introduction

Voltage-dependent potassium channels are critical for electrical activity, including repolarization of the action potential and regulation of threshold and repetitive firing behavior (Hodgkin and Huxley 1952; Connor and Stevens 1971). This can be modulated by voltage-dependent inactivation of potassium channels, which contributes to, for example, frequency-dependent action potential broadening (Aldrich et al. 1979). Analysis of inactivation has been strongly influenced by work on the *Shaker* potassium channel, which distinguished fast N-type inactivation from the (usually) slower C-type inactivation (Hoshi et al. 1991). N-type inactivation results from pore block by a cytoplasmic domain via a ball-and-chain mechanism (Hoshi et al. 1990), while C-type inactivation is strongly influenced by pore occupancy by K^+ ions or blockers (López-Barneo et al. 1993; Choi et al. 1991; Grissmer and Cahalan 1989; Baukrowitz and Yellen 1996) suggesting a pore collapse mechanism (Ogielska et al. 1995; Liu et al. 1996; Cordero-Morales et al. 2006, 2007; Cuello et al. 2010). N-type inactivation is relatively rare in other potassium channels, but C-type inactivation has been proposed for a variety of evolutionarily divergent potassium channels, including the HERG potassium channel (Smith et al. 1996) and even the voltage-independent KcsA channel of bacteria (Cordero-Morales et al. 2006).

Electronic supplementary material The online version of this article (doi:10.1007/s00232-013-9577-0) contains supplementary material, which is available to authorized users.

Q. Jamieson · S. W. Jones (✉)
Department of Physiology and Biophysics, Case Western Reserve University, Cleveland, OH 44106, USA
e-mail: swj@case.edu

Some potassium channels inactivate by mechanisms that appear to be distinct from both N- and C-type inactivation. For example, slow inactivation of the $K_V2.1$ channel is not inhibited by high extracellular K^+, and is not prevented by extracellular TEA (Klemic et al. 1998). Inactivation is strengthened by repetitive depolarization ("excessive cumulative inactivation") and has a U-shaped voltage dependence, where inactivation actually decreases upon strong depolarization. Klemic et al. (1998) proposed that these latter two observations result from preferential closed state inactivation: channels inactivate most strongly from partially activated closed states, i.e., the intermediate states along the activation pathway, while the resting closed state and the open state are relatively protected from inactivation. This form of inactivation, called U-type inactivation for its voltage dependence, is also observed for $K_V3.1$ channels and even contributes to slow inactivation in the *Shaker* IR channel (Klemic et al. 2001) and $K_V1.5$ (Kurata et al. 2001). Slow inactivation of K_V4 channels has also been proposed to involve preferential closed state inactivation, possibly related to U-type inactivation (Jerng et al. 1999; Bähring et al. 2001). One additional feature of U-type inactivation is that recovery is relatively rapid and voltage dependent, compared to C-type inactivation (Klemic et al. 2001). C-type and U-type inactivation can coexist in the same cell, but some K_V channels ($K_V2.1$ and $K_V3.1$) seem to show U-type inactivation exclusively (Klemic et al. 1998, 2001). Physiologically, cumulative U-type inactivation could play an important role in bursting activity, notably in pancreatic beta cells, where $K_V2.1$ is the predominant delayed rectifier responsible for action potential repolarization and burst termination (Jacobson et al. 2007).

In contrast to N- and C-type inactivation, little is known about the molecular mechanisms underlying U-type inactivation. Mutational analysis has identified sites in S6 (Kerschensteiner et al. 2003) and in the S5-P-loop linker (Cheng et al. 2011) that affect inactivation in $K_V2.1$, and inactivation in $K_V4.2$ may involve uncoupling of the voltage sensing S4 domain from the activation gate (Dougherty et al. 2008; Barghaan and Bähring 2009). To explore this further, we have examined effects of mutating a residue in the outer pore, Y380. This position is homologous to T449 in *Shaker,* which is a hot spot for modulating slow inactivation, probably C-type (López-Barneo et al. 1993). Mutations can speed or slow inactivation by ~100-fold (López-Barneo et al. 1993). Native K_V channels exhibit considerable diversity at this locus, which in crystal structures faces the extracellular space away from other pore-lining residues, suggesting that mutations at this site should be well tolerated. Mutations at Y380 will address whether the molecular basis of U-type inactivation is similar to C type, and will test whether a latent C-type inactivation mechanism can be revealed in $K_V2.1$. We find that mutations at this site have little effect on either activation or inactivation of $K_V2.1$, suggesting that the molecular determinants of C-type and U-type inactivation are distinct.

Materials and Methods

Cell Culture

Wild-type (WT) $K_V2.1$ channels (Frech et al. 1989) were subcloned into the pcDNA 4/TO expression vector where expression could be controlled in a time- and concentration-dependent manner with the T-Rex tetracycline-regulated expression system (Invitrogen, Grand Island, NY, USA). Mutations $K_V2.1$ Y380K, Y380A, Y380T, and Y380V were achieved with the QuikChange Site-Directed Mutagenesis Kit (Agilent Technologies, Santa Clara, CA, USA) using primers generated by the oligo synthesis service of the W.M. Keck Foundation (Yale School of Medicine, New Haven, CT, USA). Mutations were confirmed by sequence analysis (W.M. Keck Foundation). For each mutant, a stably transfected polyclonal cell line was derived from T-Rex-293 cells (Invitrogen) expressing the channel-containing pcDNA 4/TO vector using FuGENE 6 HD (Roche Applied Science, Indianapolis, IN, USA) as a transfection reagent and antibiotics as a selection mechanism as described below.

Cells were cultured in Dulbecco modified Eagle medium (DMEM; Gibco, Grand Island, NY, USA) supplemented with 10 % tetracycline-screened defined fetal bovine serum (HyClone Laboratories, Logan, UT, USA), and 1 % penicillin/streptomycin (Gibco, Grand Island, NY, USA). DMEM was further supplemented with the selective pressure of light-sensitive antibiotics Blasticidin (10 μg/mL) and Zeocin (250 μg/mL), which ensured stable transfection of pcDNA 6/TR and pcDNA 4/TO respectively. Supplemented medium was divided into 50 mL aliquots and stored in a −20 °C freezer in foil to maintain antibiotic stability and thawed before culturing. Cells were incubated at 37 °C in 95 % O_2, 5 % CO_2 in the supplemented medium, passed upon reaching 80 % confluence every 4–6 days, dispersed with trypsin, and transferred to ethanol-washed coverslips 3–4 days prior to experiments. On the day of experiments, cells were incubated with tetracycline (0.1–0.9 μg/mL) 4–6 h prior to patch clamping experiments. The concentration dependence of tetracycline incubation varied with each of the mutant constructs, possibly as the result of differences between the polyclonal cell lines generated: WT: 0.3–0.9 μg/mL, Y380T: 0.2–0.5 μg/mL, Y380V: 0.1–0.5 μg/mL, and Y380A: 0.4–0.8 μg/mL. Data throughout represent cells that

expressed current magnitudes between 4 and 20 nA at +60 mV, a range where currents were larger than endogenous levels but not large enough to introduce large series resistance error or ion depletion effects (Frazier et al. 2000). As a control for possible ion depletion effects, the reversal potential was measured for each cell and verified to be near the Nernst potential before proceeding with experiments.

Electrophysiology

T-Rex-293 cells were patched in whole-cell configuration and current traces recorded as previously described for HEK 293 cells (Khan et al. 2008). For voltage-clamp protocols measuring channel activation, data were sampled at 50 kHz following a 10 kHz analog low-pass Bessel filter. For observations of channel activation, P/4 online leak subtraction was employed. However, for observations of slow inactivation, leak-subtraction was performed offline. Pipettes with intracellular solution had resistances of 1.2–2.0 MΩ. The whole cell capacitance was 10 ± 1.2 pF and series resistance 1.9 ± 0.2 MΩ, compensated 80–90 %.

Channel activation was measured with two different protocols. The standard protocol depolarizes the membrane during P1 over a wide voltage range before repolarizing to −40 mV (Fig. 1a). The initial current amplitude at the beginning of P2 is plotted against the P1 voltage to produce the activation curve. This is done in Supplementary Fig. S2a, normalizing current amplitude to the maximum current at +60 mV.

Alternatively, channel activation can be measured by repeating the protocol in Fig. 1a but introducing a prepulse to +60 mV, which is expected to activate the same number of channels prior to studying current through channels at other voltages. Figure 1c shows this experimental protocol and resultant currents. We call this experiment the instantaneous current–voltage (IIV) protocol for its ability to measure permeation separate from gating. Figure 1d shows the IIV relationship of current through open channels. Furthermore, the initial current amplitude during the P3 pulse to −40 mV can be measured, normalized, and graphed versus the P2 voltage to produce an activation curve (Supplementary Fig. S2b).

We quantify channel activation by fitting a Boltzmann function to the activation curve. Voltage and slope parameters for both activation protocols are found in Supplementary Table S1.

The time course of channel activation was measured during P1 of the standard IV activation protocol approximating the rise of current as a monoexponential curve. The curve was fit following the sigmoidal delay in channel activation until reaching peak current for the given voltage.

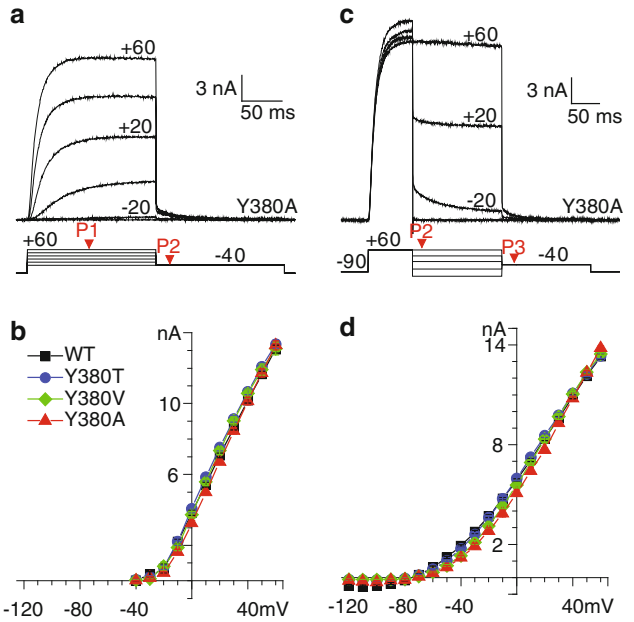

Fig. 1 $K_v2.1$ channel activation. **a** I–V protocol, mutant Y380A currents in response to depolarization from −90 mV holding potential to voltages from −40 mV to +60 mV in 10 mV increments (*P1*) in standard 5 mM KCl extracellular solution before repolarization to −40 mV (*P2*). Voltage records in 20 mV increments are shown here for cell A091020. **b** Peak currents in response to P1 are plotted versus P1 voltage to produce the I–V curve. Symbols as follows are reproduced to distinguish WT from mutant channels throughout the article: WT (*squares*), Y380T (*circles*), Y380V (*diamonds*), Y380A (*triangles*). Y380A was statistically different from WT in the range [−10, 10] mV. **c** Instantaneous I–V protocol where channels are first maximally opened with a depolarization to +60 mV then repolarized in the range −120 mV to +60 mV in 10 mV increments (*P2*) before repolarization to −40 mV (*P3*). A subset of voltages (−120, −70, −20, +20, and +60 mV) are shown here for cell A091020 **d** The peak currents in P2 from the protocol shown in **c** are plotted versus P2 voltage to produce the instantaneous I–V curve. Sample records from WT channels and other mutants can be compared in Supplementary Fig. S1. WT ($n = 10$), Y380T ($n = 15$), Y380V ($n = 10$), Y380A ($n = 9$). Y380A was statistically different from WT in the range [−60, 20] mV, Y380T in the range [−80, −60] mV, and Y380V in the range [−120, −90] and [−60, 0] mV

Recording Solutions

The intracellular pipette solution contained (mM): 120 KCl, 11 EGTA, 2 $CaCl_2$, 1 $MgCl_2$, 4 MgATP, 10 HEPES, pH 7.2, titrated with KOH. 39 mM K^+ was added from titration, yielding 159 mM total $[K^+]_i$. The extracellular bath solution contained (mM): 135 NaCl, 5 KCl, 2 $CaCl_2$, 10 HEPES, 10 glucose, pH 7.2 titrated with NaOH. Given the intracellular and extracellular potassium concentrations, the estimated Nernst potential for potassium is −88.9 mV. Osmolarity of the intracellular and extracellular solutions was approximately 300 mOsm. In experiments using 10 mM extracellular TEA-Cl, TEA^+ was

added by equimolar substitution of TEA-Cl for NaCl. The percentage block by 10 mM TEA-Cl was 20 ± 2 (Y380A, $n = 8$), 71 ± 1 (WT, $n = 6$), 18 ± 1 (Y380T, $n = 6$), and 38 ± 1 (Y380V, $n = 8$).

Model Simulation

We used a 12-state Markov model with 11 free parameters in which inactivation from closed states is allosterically coupled to voltage sensor movement (Klemic et al. 1998). Simulations of macroscopic currents were made in MATLAB Version R2011b (The MathWorks, Inc.) using the Q-matrix method (Colquhoun and Hawkes 1995). Eigenvalues and eigenvectors of the Q-matrix, containing transition rates between each of the model's 12 states, are used to find spectral matrices that determine the equilibrium occupancies for each state at a specified time and voltage. Automated parameter estimation was performed using the constrained nonlinear optimization function "fmincon" with the interior-point-convex search algorithm, minimizing the sum of absolute errors between experimental data and simulated currents. Portions of experimental data were weighted more heavily when this data contributed information critical for determining model parameters. In contrast, redundant data was deemphasized to prevent double-counting. The original model parameters (Klemic et al. 1998) were used as an initial fit. For each channel studied, two representative data sets were assembled to which the model was simultaneously fit, yielding eight total data sets and eight corresponding model solution parameter sets. In most cases, the representative data sets included data from multiple cells, which were carefully selected for internal consistency and to closely approximate average results found for each mutant (see Supplemental Material). To robustly explore parameter space, the GlobalSearch algorithm was used, which attempts to find a global minimum for a given problem by pseudorandomly exploring starting points that sample multiple basins of attraction and then optimizing these points with the fmincon subroutine. All computational work was performed locally with both the CWRU ITS High Performance Computing Cluster and laboratory computers.

Statistical Analysis

All data values are presented as mean ± standard error of the mean. A paired Student's t test was used to evaluate statistical differences between mutant and WT channels. A two-tailed p value of 0.05 was used to determine statistical significance.

Results

Y380 is not a Strong Modifier of Channel Activation

Channel activation was characterized to control for any nonspecific effects that might arise from mutations. Since inactivation is coupled to the activation process, changes to activation can affect the observed macroscopic inactivation behavior and complicate an interpretation of how a mutant affects inactivation independently from its effect on activation. WT $K_V2.1$ channels activated rapidly with a sigmoidal delay, as observed previously (Frech et al. 1989; Klemic et al. 1998), in response to a membrane depolarization to −40 mV or more (Fig. 1a). Channels were half-maximally activated near −10 mV. Currents begin to decrease over time even during only 100 ms depolarizations to +60 mV. We attribute this to slow inactivation and not intracellular ion depletion effects (Frazier et al. 2000).

The resulting current–voltage (I–V) relationship (Fig. 1b) shows that current amplitude grows nonlinearly in response to depolarization, reflecting the voltage dependence of both channel activation and ion permeation. The I–V curves reveal little difference between WT and mutant channels.

The instantaneous I–V (IIV) protocol of Fig. 1c first activates channels by depolarization to +60 mV, and then examines channel behavior upon channel repolarization. This protocol has two advantages. First, measurement of the instantaneous current upon repolarization measures the voltage dependence of ion permeation through open channels, independently from channel gating. Second, it is possible to measure channel gating kinetics at voltages where channels are not typically conductive. The resulting instantaneous I–V curve (Fig. 1d) shows permeation is nonlinear. This is consistent for WT channels and each of the mutants. While all channels had a reversal potential near −75 mV (Table 1), close to that predicted by the Nernst potential for potassium for our ionic conditions (−89 mV), each of the mutants had inward currents that showed slightly more rectification than WT channels, an unexpected observation.

Figure 2 shows the voltage dependence of activation measured at the end of the variable voltage steps (Pulse 2 of the IIV protocol or Pulse 1 of the IV protocol). Here we show the average of the two protocols' activation curves. First-order Boltzmann functions were fit to the activation curve, and the slope and voltage of half-maximal activation are presented in Table 1. Mutants activated with roughly the same voltage dependence as WT channels. The activation curve is shown separately for the IIV and IV curves (Supplementary Fig. S2a, b) with corresponding activation parameters in Supplementary Table S1. Note that the

Table 1 Activation parameters for $K_V2.1$

Channel	N	I_{+60} (nA)	V_{rev} (mV)	$V_{½}$ (mV)	k (mV)
Y380A	9	13.4 ± 1.8	−78.0 ± 1.2	−6.6 ± 1.6	9.6 ± 0.4
Y380T	15	14.7 ± 1.8	−76.7 ± 0.9	−11.8 ± 1.5	9.5 ± 0.4
$K_V2.1$ WT	10	13.1 ± 2.8	−75.9 ± 1.4	−10.9 ± 1.7	10.0 ± 0.4
Y380V	10	13.3 ± 2.0	−74.2 ± 4.1	−8.8 ± 1.2	9.7 ± 0.6

I_{+60} average of peak currents elicited by a pulse to +60 mV during the IIV protocol. The V_{rev} reversal potential is measured from interpolating the IIV curve for each cell. $V_{½}$ and k represent the voltage of half-maximal activation and slope factors, respectively, as determined from a fit of the activation curve to a first-order Boltzmann function. Values reported here are averages of the IIV and I–V activation curves for each cell (as in Fig. 2)

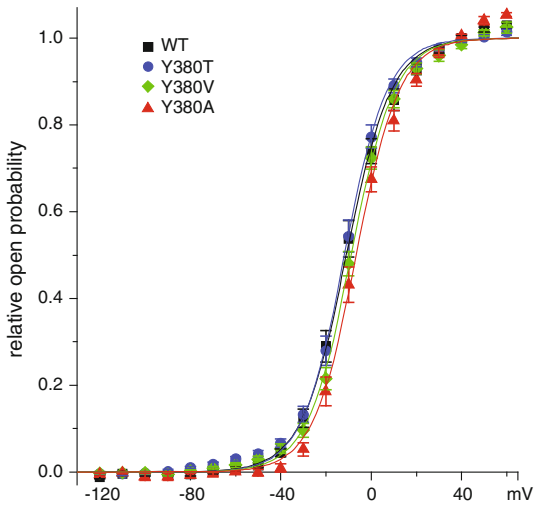

Fig. 2 Voltage dependence of channel activation. Peak tail currents during the deactivating pulse to −40 mV (P3 in the IIV protocol, or P2 in the IV protocol) are normalized to the peak tail current at +60 mV and plotted against deactivation voltage (from −120 to +60 mV), reflecting activation at a given voltage. *Solid lines* represent fits to a first-order Boltzmann function. This figure represents the average of the IV and IIV activation curves (Supplementary Fig. S2). WT ($n = 10$), Y380T ($n = 15$), Y380V ($n = 10$), Y380A ($n = 9$). Y380T was statistically different from WT in the range [−80, −60] mV and Y380V in the range [−10, 20] mV

activation curves from the IIV and IV curves differ systematically at the more negative voltages (which we call hysteresis).

We investigated whether the IIV or IV voltage-clamp protocols provided a more accurate measure of steady state activation using a longer protocol (Fig. 3b). We found that for weak depolarization, activation could be very slow and take several hundred milliseconds to fully activate. Similarly, deactivation could take more than 180 ms to reach steady state, being mindful that at longer times, the reduction in current reflects a combination of deactivation and inactivation.

We compared the current amplitude at 180 ms of the IV trace (similar to the end of P1 of Fig. 1a), the IIV trace (similar to the end of P2 of Fig. 1c), or the average of these, and compared those current measurements to the average of both records at the later time when the IV record peaked (open diamond in Fig. 3b, "peak IV"). The amplitude at 180 ms from the IIV protocol overestimated activation relative to the peak IV, and the amplitude at 180 ms from the IV protocol underestimated activation. However, the average of the activation and deactivation amplitude at 180 ms was comparable to the peak IV (Fig. 3c). All channels tested displayed some amount of hysteresis although this was small for Y380A (Supplementary Fig. S3). We conclude that neither the IV nor IIV protocols truly measured steady-state activation, but the average of the two activation curves provided a reliable estimate of channel activation.

Analyzing the time course of channel activation during the rising phase of Fig. 1a, WT channels activate with a time constant of 34.3 ± 3.8 ms ($n = 11$) at 0 mV, and the three other mutants studied activated on a similar time scale (Supplementary Table S2 and Fig. 4).

Similarly, the time course of channel deactivation was measured during the falling phase of the IIV protocol in Fig. 1c. Time constants are shown for all channels in Fig. 4. At −60 mV, WT channels deactivate exponentially with a time constant of 10.2 ± 0.8 ms ($n = 10$). The other mutants studied deactivated similarly, except the Y380A mutant exhibited notably biexponential deactivation kinetics in the range from −60 to +20 mV. The faster component, was voltage-independent with a time constant of 1.6 ± 0.3 ms at 0 mV ($n = 9$). In the voltage range where biexponential kinetics exist, the relative amplitudes of fast and slow deactivation were comparable. For example, at −20 mV, the slow component of deactivation for Y380A was 61 ± 2 % of the total ($n = 9$).

That mutations at site Y380 had little effect on the activation process suggests that any effects on macroscopic inactivation will reflect changes in the inactivation mechanism itself.

Y380 Mutations Weakly Modify Channel Inactivation

Mutations of the outer pore residue T449 in *Shaker* IR channels led to dramatic changes in the kinetics of

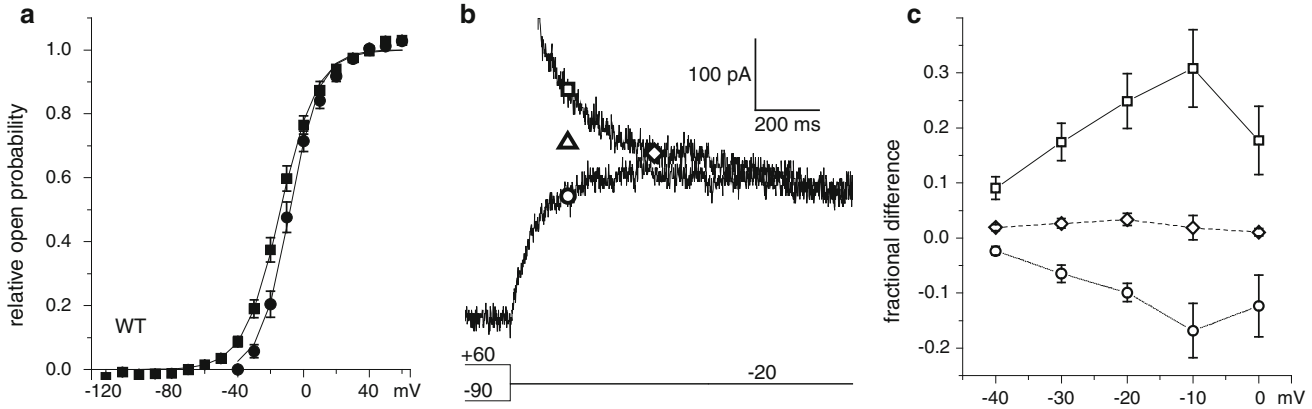

Fig. 3 Hysteresis of channel activation. **a** The voltage dependence of channel activation is shown for WT channels as measured from the IIV protocol (*squares*) and the IV protocol (*circles*) revealing a hysteresis in the two activation curves. **b** Superimposed records recorded using IV and IIV protocols (as in Fig. 1a, c) but with longer voltage steps, shown at −20 mV, where hysteresis is strong. The *square* and *circle* mark the currents at 180 ms, the time when the −40 mV step to measure channel activation began for the protocol of Fig. 1. The *triangle* shows the average of these 2 currents. The *diamond* marks the average of the current during the IIV and IV steps at the time of peak in the IV current (peak IV). Cell WT B100708. **c** The peak IV current was subtracted from the current amplitudes measured at 180 ms (IIV protocol, IV protocol, and average; symbols as in **b**). This analysis was repeated for all mutants (Supplementary Fig. S3)

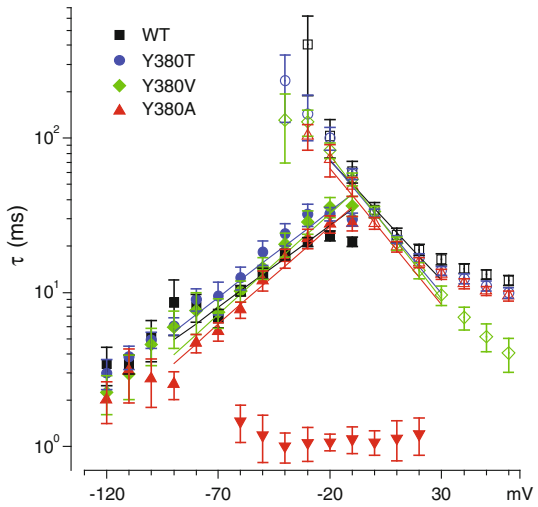

Fig. 4 Kinetics of channel activation and deactivation. For deactivation (−120 to −10 mV), time constants are measured from exponential fits to the deactivation phase of the IIV protocol (Fig. 1c, P2). Currents were fitted to a single exponential, except for Y380A, where time constants are shown from a biexponential fit (*triangles,* slow component; *inverted triangles,* fast component). For activation (−40 to +60 mV), time constants are measured from monoexponential fits to the activation phase of the IV protocols (Fig. 1a, P1) and are displayed here as *open symbols. Lines* represent logarithmic fits to either the activation or deactivation time constants. WT ($n = 10$), Y380T ($n = 15$), Y380V ($n = 10$), Y380A ($n = 10$). Y380V was statistically different from WT in the range [20, 60] mV

inactivation depending on the amino acid expressed (López-Barneo et al. 1993). Figure 5 shows representative traces from channels expressing mutations at the site corresponding to *Shaker* IR T449: (A) $K_V2.1$ Y380A, (B) WT Y380 $K_V2.1$ channels, (C) Y380T, and (D) Y380V.

The inactivation rate, measured from exponential fits to the decay of current during 10-s steps from 0 to +60 mV, was not significantly affected by any of the mutations (Supplementary Table S2). Furthermore, none of the mutants systematically exhibited biexponential inactivation kinetics that could be ascribed to distinct C- and U-type inactivation mechanisms.

Figure 5e shows that the voltage-dependence of inactivation was weakly affected by each of the mutants. Specifically, all inactivated most strongly in the middle of the voltage range. Furthermore, inactivation developed in roughly the same voltage range and to the same extent.

To examine inactivation at voltages that produce little channel activation, test pulses were given following depolarizations of variable length. Figure 6a illustrates this protocol for mutant Y380T with conditioning pulses to −40 mV. Inactivation is slow in this voltage range and can take many seconds to develop. Inactivation is well-described by a monoexponential fit and is 30.7 ± 4.0 % complete after 30 s (Supplementary Fig. S4f). Repeating the protocol at −10 mV (a voltage where activation is half-maximal) shows that inactivation is faster, more complete, well-described by a monoexponential fit, and is 76.7 ± 2.7 % complete after 10 s (Supplementary Fig. S4f). The time constant of inactivation described by this protocol (3.7 ± 0.2 s, $n = 12$) was close to that measured with the protocol of Fig. 5 (3.8 ± 0.2 s, $n = 10$).

The protocol of Fig. 6a was repeated for each of the mutants (Fig. 6b, c, and Supplementary Fig. S4). Inactivation at −10 mV (Fig. 6b) was slightly but significantly slower in all 3 mutants compared to WT. Inactivation at −40 mV (Fig. 6c) was more complete in WT and Y380A

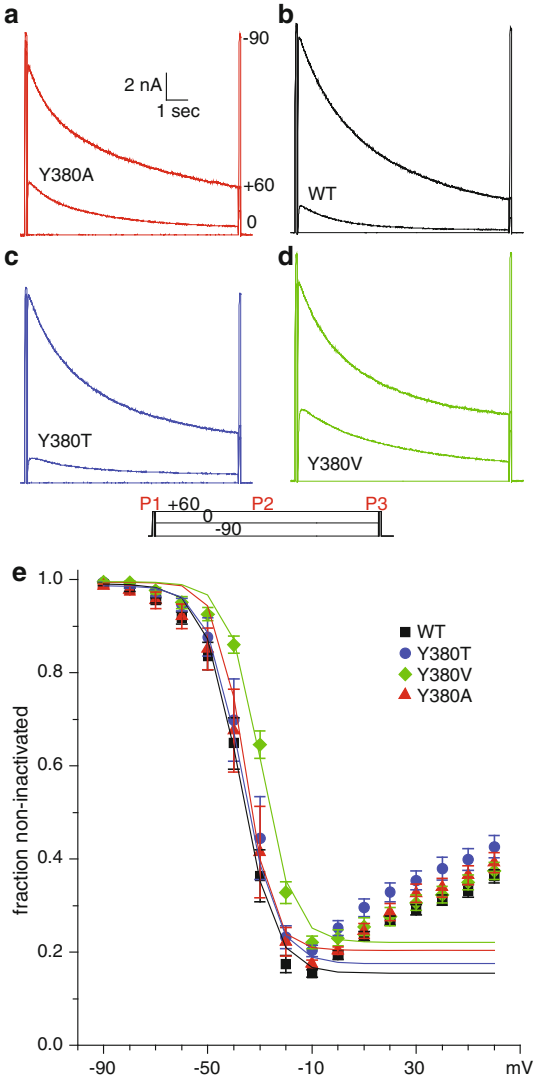

Fig. 5 Channel inactivation. The three-pulse protocol examines channel availability after a 10-s inactivating pulse (P2) depolarizing channels from −90 to +60 mV in 10 mV increments. Only a subset of voltages is shown here at −90, 0, and +60 mV for: **a** Y380A cell B100728, **b** WT cell D100722, **c** Y380T cell C100812, and **d** Y380V cell C090702. The current and time scale in **a** is the same for **a–d**. **e** The ratio of current elicited during a test pulse to +60 (P3) compared to the control pulse to +60 (P1) is plotted. *Solid curves* are fits to a first-order Boltzmann function. Y380A ($n = 5$), WT ($n = 7$), Y380T ($n = 7$), Y380V ($n = 7$). Y380V was statistically different from WT in the range [−80, 0] mV, Y380T at −10 mV and in the range [10, 50] mV, and Y380A at −20, +50, and +60 mV

channels (55 and 50 % complete, respectively, at 30 s; compared to 31 and 27 % for Y380T and Y380V, respectively) but still fit reasonably well by a single exponential (Supplementary Table S3). Note that −40 mV is in the steep part of the inactivation curve (Fig. 5e), where small changes in voltage can have large effects on the extent of inactivation.

We studied recovery from inactivation with the protocol of Fig. 7a. After a 5-s inactivating pulse to 0 mV, channels recover from inactivation over a wide voltage range (−140 to −60 mV). In WT channels, recovery from inactivation is well-fit by a single exponential at all recovery voltages. Recovery is also fast near the resting potential. At −90 mV, the time constant of recovery was 1.5 ± 0.2 s ($n = 11$), and recovery was 90 % complete after about 10 s. Figure 7a shows recovery at −90 mV in mutant Y380T. Recovery is strongly voltage dependent in Y380T (Fig. 7b), At–140 mV, $\tau_{rec} = 96.7 \pm 10.5$ ms ($n = 7$), but recovery is slower and less complete at more positive voltages (at −60 mV, $\tau_{rec} = 3.9 \pm 0.7$ s, $n = 5$). Recovery was well-described by a monoexponential fit all voltages. All channel constructs had strongly voltage-dependent recovery from inactivation (Fig. 7c–e). Currents for each channel in response to the protocol of Fig. 7a can be seen in Supplementary Fig. S5. Supplementary Table S4 quantifies these observations showing time constants of recovery from inactivation calculated from monoexponential fits to smooth curves in Fig. 7b–e. One unexpected difference among the channels is that recovery was 2- to 3-fold faster in the Y380T and Y380V mutants (Supplementary Fig. S6).

Figure 8 summarizes all the kinetic data collected from experiments examining recovery from inactivation, onset of inactivation at weak depolarization, and onset of inactivation at more strongly depolarized voltages. The figure demonstrates the broad temporal range of inactivation in $K_V2.1$ and the mutants, strongly reflected not only by the voltage-dependence of recovery from inactivation at negative voltages, but also by the slow rate of inactivation at weakly depolarized voltages where few channels open.

TEA Fails to Inhibit Inactivation

As described in the Introduction, extracellular tetraethylammonium (TEA) application has been shown to inhibit C-type inactivation by a "foot-in-the-door" mechanism (Grissmer and Cahalan 1989; Choi et al. 1991; López-Barneo et al. 1993). Though TEA has no effect on inactivation kinetics of WT $K_V2.1$ channels (Klemic et al. 1998), examining how TEA affects Y380 mutants will further test if any of these mutants can reveal a latent C-type inactivation in $K_V2.1$.

The kinetics of inactivation are unaffected by the presence of 10 mM TEA (open triangles) at either −10 mV (Fig. 9a) or +60 mV (Fig. 9b). Channel mutant Y380A inactivated with a time constant of 2.94 ± 0.53 s ($n = 4$) at +60 mV in control conditions versus 2.86 ± 0.78 s ($n = 4$) in the presence of 10 mM TEA. The voltage-dependence and extent of inactivation were also unaffected by 10 mM TEA treatment, and the fraction of noninactivating channels is not affected by TEA at either −10 mV (Fig. 9c) or +60 mV (Fig. 9d).

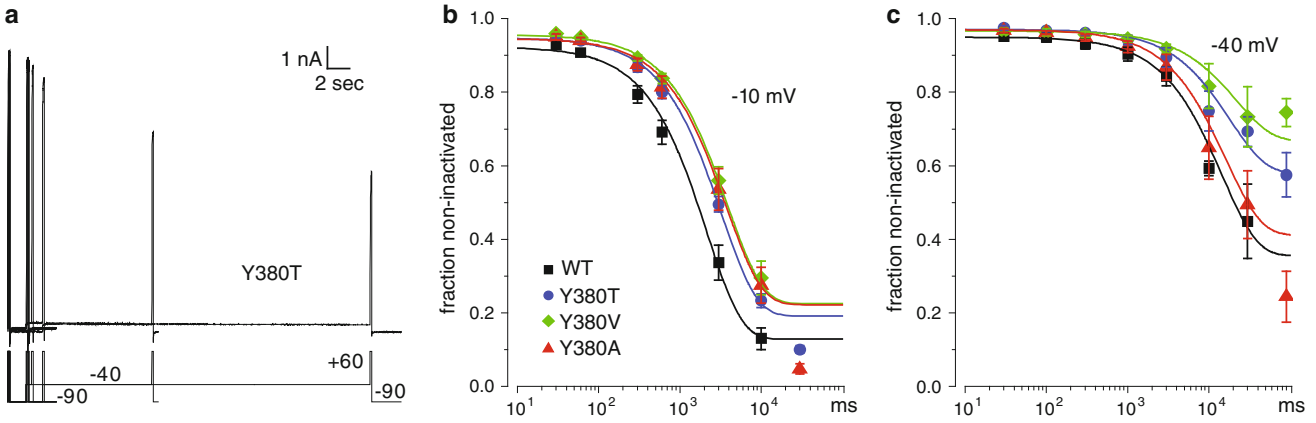

Fig. 6 Inactivation with weak depolarization. **a** Protocol: Y380T channels were depolarized to +60 mV (prepulse) to measure channel availability before a variable-length pulse to −40 mV to inactivate channels. This was followed by a second test pulse to +60 mV (postpulse) to measure the remaining noninactivated channels. Y380T cell G100104. **b** Time course of inactivation at −10 mV. The fraction of noninactivated channels was calculated as the ratio of the postpulse to prepulse for the protocol shown in **a**. Y380A and Y380T are statistically different from WT at all times, Y380V at all times except 3,000 and 10,000 ms. **c** Time course of inactivation at −40 mV. Y380V was statistically different from WT at 3,000 and 10,000 ms. Smooth curves represent monoexponential fits to the data. Y380A ($n = 7$), WT ($5 \leq n \leq 6$), Y380T ($10 \leq n \leq 12$), Y380V ($8 \leq n \leq 12$). The protocol in **a** was repeated for all mutants (Supplementary Fig. S4)

Taken together, TEA was unable to affect the proportion of inactivating channels or the speed with which mutants inactivate at voltages that might favor U-type (−10 mV) or C-type inactivation (+60 mV).

Kinetic Modeling Suggests Channels Exhibit Weak Open-state Inactivation

A 12-state allosteric model (Supplementary Fig. S7) for inactivation of $K_V2.1$ channels (Klemic et al. 1998) was used to simulate WT channels and each of the study's mutants Y380A, Y380T, and Y380V. The model, which permits inactivation from both closed and open channels, tested how each of the pore mutants might affect the channel's preference for closed- versus open-state inactivation, and also whether mutants might affect other channel parameters. Parameter estimation was performed with MATLAB using an automated global optimization routine.

Model parameters for WT channels were compared to those published previously (Klemic et al. 1998) to test the accuracy of parameters fit by hand versus those determined computationally. Of the model's 11 free parameters, all were within an order of magnitude of the previously published values for WT $K_V2.1$ channels. The two WT data sets modeled produced two very different parameter sets suggesting that the final parameters were not well-determined. This result was mirrored in the Y380 mutants and is explored further in Supplementary Material. The apparent charge associated with voltage sensor deactivation appeared to be smaller than originally published: a "z" value of −0.20 or −0.42 versus the originally published value of −0.54 (Klemic et al. 1998). The apparent charges associated with voltage-sensor activation and channel closing were nearer to previously published values. Some parameters were very well-determined. The allosteric factor "f," which describes how strongly inactivation is favored by voltage-sensor activation, was modeled to be 0.16 or 0.17, which is near the published value of 0.17. Furthermore, the allosteric factor describing the amount of inactivation occurring from open channels "g" was modeled to be 0.01 and 0.04 versus the published value of 0.02 confirming the interpretation that open-state inactivation is very weak in WT $K_V2.1$ channels. Both of the parameter sets for WT channels can be found in Supplementary Table S5.

The model was able to describe both WT and mutant data equally well, reproducing the key features of U-type inactivation. Notably, simulated currents exhibited a strong U-shaped voltage-dependence of inactivation, maximal near −10 mV, slow weakly voltage-dependent inactivation, and strongly voltage-dependent recovery from inactivation (Fig. 10). The model, however, was unable to reproduce the hysteresis observed in measurement of channel activation (Fig. 3), the biexponential deactivation kinetics of Y380A (Fig. 4) or the subtle nonmonoexponential kinetics of inactivation observed in some experiments. Encouragingly, the model was able to reproduce the faster recovery from inactivation seen in the Y380T and Y380V mutants (Supplementary Fig. S8); however, there was no clear correspondence between faster recovery kinetics and specific model parameters.

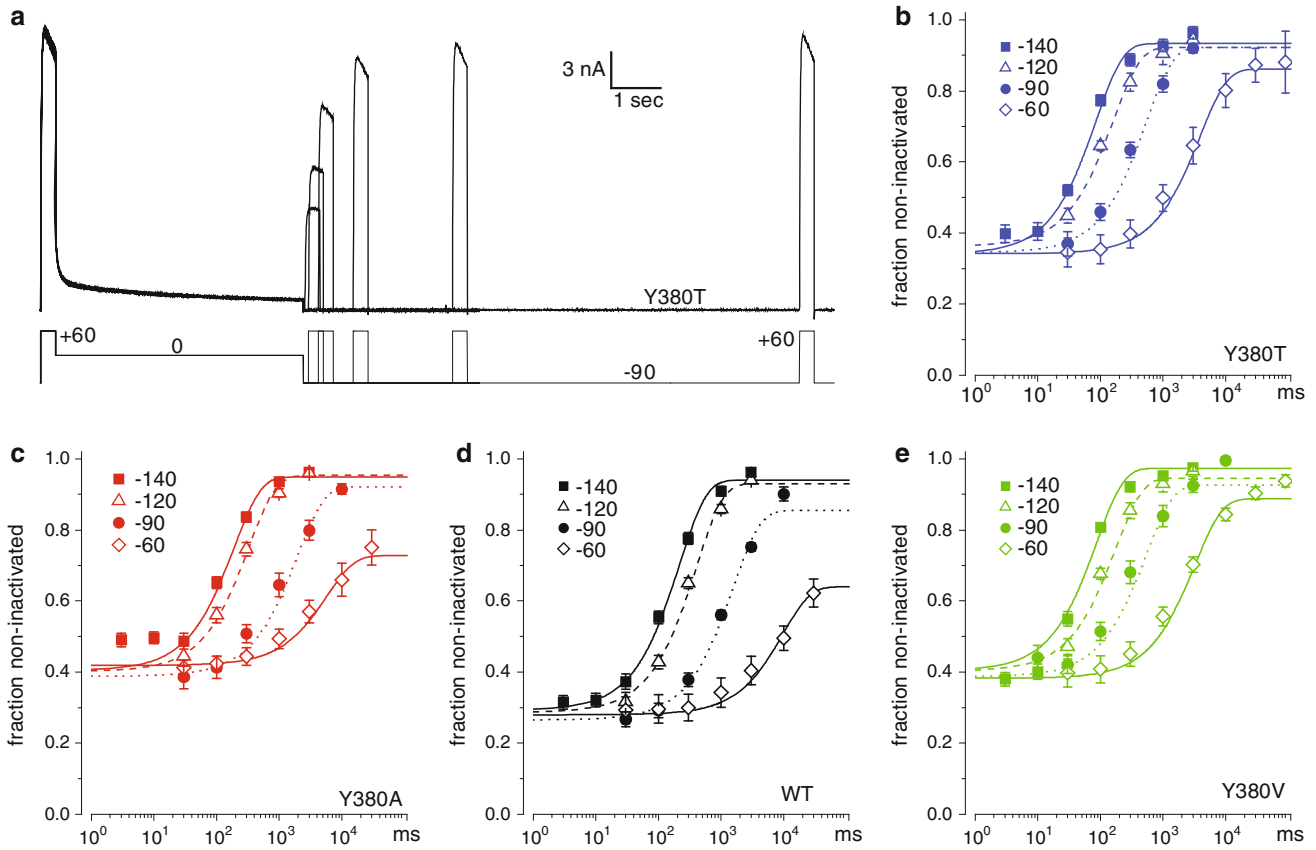

Fig. 7 Recovery from inactivation. **a** Protocol: Y380T channels were depolarized to +60 mV (prepulse) to measure channel availability before a 5-s inactivation pulse to 0 mV. Channels then recovered from inactivation for a variable duration at −90 mV before the fraction of noninactivated channels was measured with a second pulse to +60 mV (postpulse). Y380T cell A090326. **b** The fraction of available Y380T channels, calculated as the ratio of the postpulse to prepulse, plotted vs. the time of recovery, for four recovery voltages: −140 mV (*solid squares*), −120 mV (*open triangles*), −90 mV (*solid circles*), or −60 mV (*open diamonds*). This time-dependence of recovery is shown similarly for **c** Y380A, **d** WT, and **e** Y380V channels ($5 \leq n \leq 11$). *Smooth curves* represent monoexponential fits to the data. The protocol was repeated for all mutants. (See Supplementary Fig. S5 for current records, and Supplementary Fig. S6 to compare mutants at each voltage)

The automated parameter estimation routine found parameters for each of the eight assembled data sets that were variable not only across different mutants, but also for data sets belonging to the same mutant (Supplementary Material). While parameter "f" appeared to be well determined, the amount of open-state inactivation (parameter "*g*") varied from a value as small as 0.0130 (WT Y3) to as large as 0.1706 (Y380A A2) with an average of $g = 0.08 \pm 0.02$ ($n = 8$) compared to $g = 0.02$ (Klemic et al. 1998). Some data sets suggested quantitatively more open-state inactivation than originally proposed (Klemic et al. 1998), but all parameter sets exhibit strong preferential closed-state inactivation ($g < 0.2$).

Discussion

T449 was identified as a hotspot for C-type inactivation in *Shaker* (López-Barneo et al. 1993). This site, near the outer mouth of the pore, exhibits high variability across native K_V channels, suggesting it may be a region of functional diversity (MacKinnon and Yellen 1990). In $K_V2.1$, the analogous residue is a tyrosine (Y380), an amino acid when substituted in *Shaker* IR slowed inactivation tenfold (López-Barneo et al. 1993). The present study tested whether similar mutations at the equivalent site in $K_V2.1$ could reproduce the effects on inactivation seen in *Shaker* IR.

Three mutations were made at site $K_V2.1$ Y380: one that reproduces the native residue of *Shaker* (threonine), one that accelerated inactivation in *Shaker* IR (alanine), and one that slowed inactivation (valine).

Activation

We examined the effect of these mutations on activation first, since any effects on inactivation could be the result of changes in channel activation, as the voltage dependence of inactivation is thought to result from coupling to the

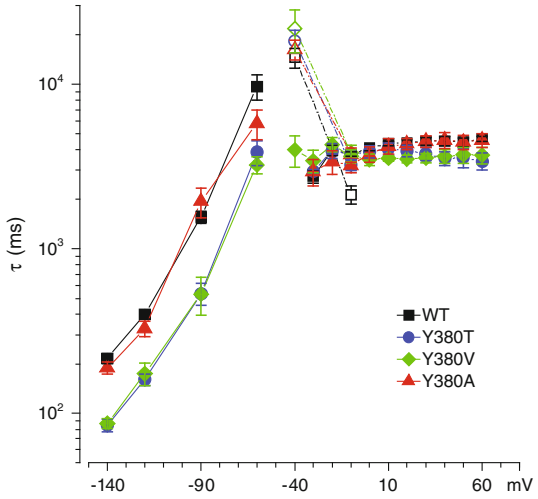

Fig. 8 Kinetics of inactivation and recovery. From −140 to −60 mV, time constants of recovery from inactivation are plotted vs. the recovery voltage. Solid symbols identifying channel mutants are as previously described. At −40 and −10 mV, time constants of onset of inactivation from the protocol of Fig. 6a are plotted vs. inactivating voltage and are shown as open symbols. From −40 to +60 mV, time constants of inactivation are plotted vs. inactivating voltage and are shown as *solid symbols*. Time constants reflect monoexponential fits to data as in Fig. 7b–e (recovery from −140 to −60 mV), Fig. 6b, c (onset at −40 and −10), and Fig. 5a–d, Pulse 2 (onset from −40 to +60 mV). Y380A ($5 \le n \le 9$), WT ($4 \le n \le 10$), Y380T ($5 \le n \le 7$), Y380V ($7 \le n \le 10$). Y380A was statistically different from WT at −10 mV, Y380T in the range [−140, −90] mV and at −10 mV, and Y380V in the range [−140, −60] and [10, 30] mV

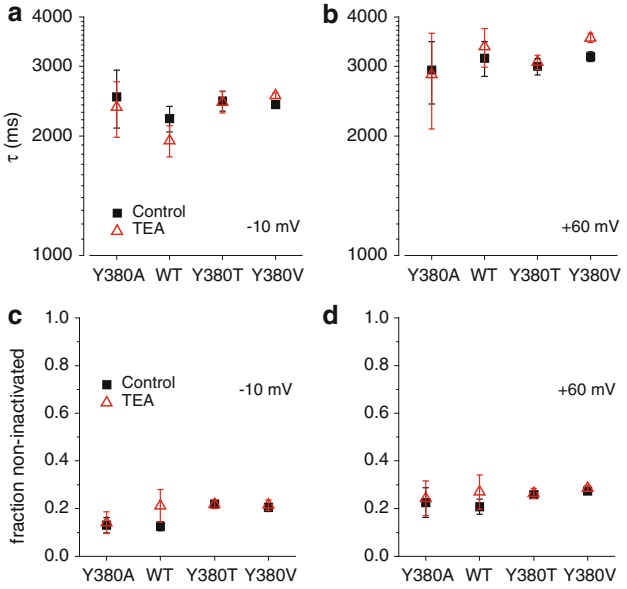

Fig. 9 Effect of external TEA. A total of 10 mM extracellular TEA-Cl was added by equimolar substitution of TEA-Cl for NaCl. The inactivation protocol of Fig. 5 was repeated first as a control, again with 10 mM TEA-Cl, and again after washout to test for reversibility. Time constants from monoexponential fits are shown for control (averaged with washout, *solid squares*) and 10 mM TEA (*open triangles*) at **a** −10 mV and **b** +60 mV. The voltage dependence of inactivation was measured from the ratio of test pulses as in Fig. 5e for control, TEA, and washout. The fraction of noninactivated channels is shown for control (averaged with washout, *solid squares*) and 10 mM TEA (*open triangles*) at **c** −10 mV and **d** +60 mV

activation process and this relationship is built into our allosteric model of inactivation (Supplementary Fig. S7). Because of the sensitivity of inactivation to the activation process, we therefore chose to do a thorough characterization of activation.

We found that none of the mutants shifted the voltage-dependence of activation as determined by a voltage-by-voltage comparison to WT channels (Fig. 2). Furthermore, the time course of activation and deactivation were similar for all of the mutants, except for the biexponential deactivation kinetics of Y380A (Fig. 4). The result of our comprehensive activation study, while negative, is surprising given mutations more often have some effect rather than none.

The effect of the Y380A mutant to induce biexponential channel deactivation is a novel observation. Faster deactivation resulted in the IIV protocol reaching steady state more quickly, reducing the difference in activation measured from the IV and IIV protocols (Supplementary Fig. S3).

Inactivation

Mutations of T449 strongly affect slow inactivation of *Shaker,* and similar effects are seen in some mammalian K_V1 channels, notably $K_V1.3$ (Nguyen et al. 1996) and $K_V1.4$ channels (Rasmusson et al. 1995). On the other hand, slow inactivation of $K_V1.5$ channels is weakly modified by pore mutation or by high extracellular potassium (Fedida et al. 1999), and $K_V1.5$ can exhibit U-type inactivation, at least following mutations to the N-terminal region (Kurata et al. 2005). One interpretation is that mammalian K_V1 channels, like *Shaker,* can exhibit a mixture of C- and U-type inactivation. Inactivation of the distantly related HERG channel is also sensitive to mutations at the equivalent to *Shaker* 449, and has been suggested to be C-type inactivation (Smith et al. 1996). Further study is needed, but it seems possible that sensitivity to mutation at this position can be an additional criterion to distinguish C- from U-type inactivation.

None of the mutations could reproduce the dramatic effects on inactivation seen in *Shaker* (López-Barneo et al. 1993). We conclude that $K_V2.1$ Y380 is not a strong determinant of inactivation in $K_V2.1$, unlike T449 is in *Shaker* IR. In particular, the observation that $K_V2.1$ Y380A (Fig. 5a) does not mimic the 100-fold increase in inactivation rate observed for *Shaker* T449A suggests that even a mutation that strongly enhances C-type inactivation in *Shaker* cannot produce C-type inactivation in $K_V2.1$. This

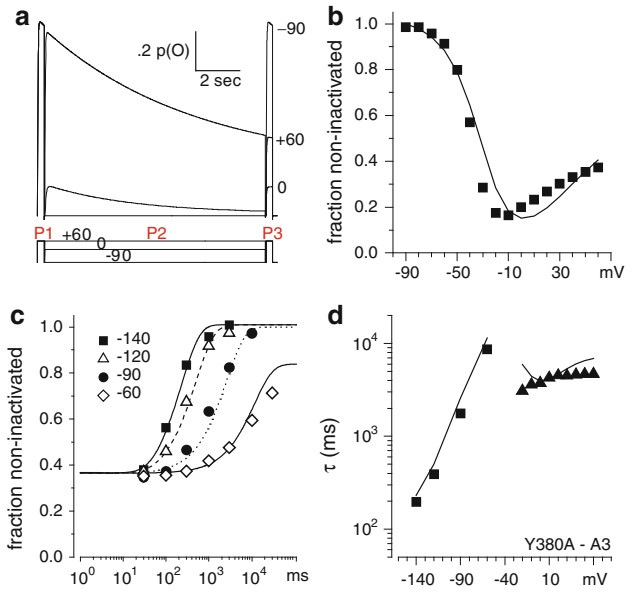

Fig. 10 An allosteric model reproduces key features of U-type inactivation. Simulated currents are shown from a fit to a Y380A mutant data set (parameters provided in Supplementary Table S5, data set Y380A A3). **a** Inactivation, simulated from the protocol in Fig. 5a–d. **b** The U-shaped voltage dependence of inactivation measured from the ratio (P3/P1) of currents in **a** (*solid curve*), compared to A3 data (*squares*). **c** The time course of recovery from inactivation as in Fig. 8 as simulated (*curves*) vs. A3 data (*symbols*). **d** Fitted time constants for recovery from inactivation (*squares*) and development of inactivation (*triangles*) for data set A3 as in Fig. 8 with modeled time constants (*curves*). Fits to other data sets are shown in Supplementary Fig. S11–S18

is further evidence that $K_V2.1$ lacks C-type inactivation as it exists in *Shaker* IR, and that C-type and U-type inactivation have different molecular determinants.

All mutants showed strong closed-state inactivation (Fig. 6a and Supplementary Fig. S4). At–40 mV, where only about 5 % of channels are activated, the extent of inactivation varied for each mutant (Fig. 6c). Y380V inactivated only 27 % after 90 s versus 58 % for WT channels. Since this is on the steepest phase of the inactivation curve (Fig. 5e), small changes in voltage dependence, or in coupling of inactivation to activation, can explain this variability.

In *Shaker,* C-type inactivation recovers slowly and is weakly voltage dependent, while recovery from U-type inactivation can be rapid and is strongly voltage dependent (Klemic et al. 2001), similar to $K_V2.1$ (Klemic et al. 1998). For $K_V2.1$, we find that recovery was monoexponential for all mutants, with no evidence for a slow, voltage-independent component to recovery. This supports the idea that C-type inactivation is absent in $K_V2.1$.

However, recovery from inactivation was accelerated in the Y380T and Y380V mutants, both of which had strongly voltage-dependent recovery from inactivation (Fig. 8). We interpret this as faster recovery from U-type inactivation. The faster recovery could shift the inactivation-recovery equilibrium, contributing to the small shift of the inactivation curve to more positive voltages in Y380V (Fig. 5e) and the reduction in inactivation at −40 mV (Fig. 6c). Y380 is distant from regions currently implicated in closed-state inactivation, namely the S4–S5 linker and S6, so the significance of these effects for the molecular mechanism of U-type inactivation is not clear.

The state of the outer pore can affect inactivation in both *Shaker* IR and $K_V2.1$. In *Shaker* IR, high K^+ or TEA inhibit inactivation by a foot-in-the-door mechanism. In contrast, inactivation was slightly faster in high K^+ for WT $K_V2.1$, and TEA had no effect (Klemic et al. 1998). In this study, we confirm this result for all of the mutations (Fig. 9); however, this conclusion is limited because 10 mM TEA blocked only 20–40 % of the current for the mutated channels. Taken together, this suggests that the outer pore region of $K_V2.1$ must influence inactivation differently than in *Shaker* IR.

Because mutations had little effect on inactivation in $K_V2.1$, we conclude that $K_V2.1$ does not exhibit C-type inactivation, even when mutations that should enhance C-type inactivation are introduced. Furthermore, the molecular determinants of C- and U-type inactivation must be different.

Allosteric Model

We adapted our previously published allosteric model for $K_V2.1$ channels (Klemic et al. 1998) in MATLAB to permit automated estimation of the model's 11 parameters using the Q-Matrix method (Colquhoun and Hawkes 1995). This model can produce a good quantitative and qualitative description of the experimental data. There are some relatively minor features that cannot be described by the model, notably the biexponential deactivation kinetics observed for Y380A, and a variably biexponential time course for inactivation for all channel constructs. The hysteresis in the activation curve, resulting from unexpectedly slow activation at the foot of the activation curve, was also not reproduced by the model. Overall, we believe that continuing to interpret gating of $K_V2.1$ in terms of the Klemic et al. (1998) model is well justified.

We conclude that inactivation occurs preferentially from partially activated closed states, in terms of the model. The best fit values for the parameter g, estimating open-state inactivation, ranged from 0.01 to 0.17, compared to 0.02 in the model of Klemic et al. (1998). A value of $g = 0$ allows inactivation exclusively from closed states, while $g = 1$ allows inactivation from the open state (O_4) and nearest closed state (C_4) at the same rate; preferential open state inactivation would require $g > 1$. This means that the last

closed-inactivated state, I_4, is favored over C_4 by a factor of g^2, compared to the equilibrium between the open inactivated state I_4* versus O_4. If we constrained g to be >0.3, or to be equal to 0, good fits could not be obtained (calculations not shown). This means that preferential closed state inactivation is strong, but not absolute, as including a small amount of open state inactivation describes the data more accurately. For example, in one of the Y380A data sets, model simulations at steady state at +60 mV predicts that 23 % of channels are open (O_4), 67 % are in the nearest closed-inactivated state (I_4), and 9 % are in the open-inactivated state (I_4*). At 0 mV, 91 % are in closed-inactivated states, 4 % are open, and 1 % open-inactivated. But 3 of the 8 best-fit parameter sets showed stronger inactivation from open channels at steady state (e.g., 10 % at 0 mV and 36 % at +60 mV, data set Y380T T3). However, even these models predicted preferential closed-state inactivation at 0 mV.

The model simulations suggest that U-type inactivation in K_V2.1 consists of a mix of both open- and closed-state inactivation with preferential inactivation from closed states throughout the voltage range. In this view, open-state and closed-state inactivation of K_V2.1 are part of a single U-type inactivation process, not two qualitatively different inactivation mechanisms.

Structure–function Relationships for U-type Inactivation

Since the initial characterization of U-type inactivation in WT K_V2.1 channels (Klemic et al. 1998), few studies have attempted to describe its molecular basis. A chimera in which the amino-terminal domain of K_V1.5 (including the T1 domain) was attached to a K_V2.1 transmembrane core eliminated the U-shaped voltage-dependence of inactivation and drastically reduced the extent of inactivation (Kurata et al. 2002), while the reverse chimera imparted a U-shape in K_V1.5 channels. The T1 domain represents a potentially interesting target for future study.

A point mutation P410T in the widely conserved PxP (proline-x-proline) motif of the S6 transmembrane domain of K_V2.1 enhanced closed-state inactivation, and slowed inactivation at more positive voltages (Kerschensteiner et al. 2003). This is reminiscent of effects of coexpression with the "silent" K_V5.1 subunit, which lacks the second proline in that motif. We have preliminary results with the same mutation (data not shown), which reveal slower activation and a left-shifted inactivation curve with a deeper U shape, but this may result in part from a shift in channel activation to more negative voltages. This emphasizes that careful examination of channel activation is necessary to draw conclusions about whether a mutation directly affects the channel inactivation process.

Most recently, a mutation introduced in the K_V2.1 S5-P-loop linker (E352C) greatly reduced the U shape of the inactivation curve (Cheng et al. 2011). This was interpreted as elimination of U-type inactivation, but the model for E352C used $g = 0.39$, indicating that preferential closed state inactivation is reduced but not eliminated (noting that parameters were estimated by eye in that study). Curiously, U-shaped inactivation was restored in E352C by DTT, or by a C232 mutation in S2, suggesting a disulfide bond between the S2 and S5-P-loop domains inhibits U-type inactivation (Cheng et al. 2011). It does not appear that inactivation in E352C is C-type, as it is not affected by high extracellular K^+. Recovery from inactivation was still rapid and strongly voltage dependent in E352C. We suspect that this mutation has a quantitative effect on U-type inactivation, rather than eliminating or replacing the U-type mechanism.

Our results demonstrate that mutations of Y380 have little effect on U-type inactivation However, this negative result allows a strong positive conclusion, that the molecular determinants of C-type and U-type inactivation are different, and that K_V2.1 lacks C-type inactivation as it exists in other channels where pore mutations can strongly modulate inactivation. Furthermore, in addition to the established pharmacological and voltage protocols used to separate C- vs U-type inactivation, we suggest that pore mutation may be an additional criterion to help distinguish between C- and U-type inactivation mechanisms. However, the molecular and structural basis of U-type inactivation in K_V2.1 channels remains to be determined.

Acknowledgments This work was supported in part by National Institutes of Health grant NS24771 to S.W. Jones. We thank the CWRU ITS High Performance Computing Cluster for computational time. We acknowledge the invaluable assistance of Dr. Carlos A. Obejero-Paz in establishing polyclonal cell lines for each of the K_V2.1 Y380 mutants. We also thank Dr. Eckhard Ficker for the gift of the pcDNA3 expression vector containing the WT K_V2.1 channel. We are also grateful for the insightful discussion and thoughtful critique provided by Dr. Diana Kunze, Dr. Sudha Chakrapani, and Dr. Jessica Berthiaume.

Conflict of interest The authors report no conflicts of interest.

References

Aldrich RW Jr, Getting PA, Thompson SH (1979) Mechanism of frequency-dependent broadening of molluscan neurone soma spikes. J Physiol (Lond) 291:531–544

Bähring R, Boland LM, Varghese A, Gebauer M, Pongs O (2001) Kinetic analysis of open- and closed-state inactivation transitions in human Kv4.2 A-type potassium channels. J Physiol 535 (pt 1):65–81

Barghaan J, Bähring R (2009) Dynamic coupling of voltage sensor and gate involved in closed-state inactivation of Kv4.2 channels. J Gen Physiol 133:205–224

Baukrowitz T, Yellen G (1996) Use-dependent blockers and exit rate of the last ion from the multi-ion pore of a K^+ channel. Science 271(5249):653–656

Cheng YM, Azer J, Niven CM, Mafi P, Allard CR, Qi J, Thouta S, Claydon TW (2011) Molecular determinants of U-type inactivation in Kv2.1 channels. Biophys J 101:651–661

Choi KL, Aldrich RW, Yellen G (1991) Tetraethylammonium blockade distinguishes two inactivation mechanisms in voltage-activated K^+ channels. Proc Natl Acad Sci USA 88:5092–5095

Colquhoun D, Hawkes AG (1995) A Q-matric cookbook. How to write only one program to calculate the single-channel and macroscopic predictions for any kinetic mechanism. In: Sakmann B, Neher E (eds) Single-channel recording, 2nd edn. Plenum Press, New York, pp 589–633

Connor JA, Stevens CF (1971) Inward and delayed outward membrane currents in isolated neural somata under voltage clamp. J Physiol (Lond) 213:1–19

Cordero-Morales JF, Cuello LG, Zhao Y, Jogini V, Cortes DM, Roux B, Perozo E (2006) Molecular determinants of gating at the potassium-channel selectivity filter. Nat Struct Mol Biol 13:311–318

Cordero-Morales JF, Jogini V, Lewis A, Vasquez V, Cortes DM, Roux B, Perozo E (2007) Molecular driving forces determining potassium channel slow inactivation. Nat Struct Mol Biol 14:1062–1069

Cuello LG, Jogini V, Cortes DM, Perozo E (2010) Structural mechanism of C-type inactivation in K(+) channels. Nature 466(7303):203–208

Dougherty K, De Santiago-Castillo JA, Covarrubias M (2008) Gating charge immobilization in Kv4.2 channels: the basis of closed-state inactivation. J Gen Physiol 131:257–273

Fedida D, Maruoka ND, Lin SP (1999) Modulation of slow inactivation in human cardiac Kv1.5 channels by extra- and intracellular permeant cations. J Physiol (Lond) 515:315–329

Frazier CJ, George EG, Jones SW (2000) Apparent change in ion selectivity caused by changes in intracellular K^+ during whole-cell recording. Biophys J 78:1872–1880

Frech GC, VanDongen AM, Schuster G, Brown AM, Joho RH (1989) A novel potassium channel with delayed rectifier properties isolated from rat brain by expression cloning. Nature 340(6235):642–645

Grissmer S, Cahalan M (1989) TEA prevents inactivation while blocking open K^+ channels in human T lymphocytes. Biophys J 55:203–206

Hodgkin AL, Huxley AF (1952) Currents carried by sodium and potassium ions through the membrane of the giant axon of *Loligo*. J Physiol (Lond) 116:449–472

Hoshi T, Zagotta WN, Aldrich RW (1990) Biophysical and molecular mechanisms of *Shaker* potassium channel inactivation. Science 250(4980):533–538

Hoshi T, Zagotta WN, Aldrich RW (1991) Two types of inactivation in *Shaker* K^+ channels: effects of alterations in the carboxy-terminal region. Neuron 7:547–556

Jacobson DA, Kuznetsov A, Lopez JP, Kash S, Ammala CE, Philipson LH (2007) Kv2.1 ablation alters glucose-induced islet electrical activity, enhancing insulin secretion. Cell Metab 6:229–235

Jerng HH, Shahidullah M, Covarrubias M (1999) Inactivation gating of Kv4 potassium channels. Molecular interactions involving the inner vestibule of the pore. J Gen Physiol 113:641–659

Kerschensteiner D, Monje F, Stocker M (2003) Structural determinants of the regulation of the voltage-gated potassium channel Kv2.1 by the modulatory α-subunit Kv9.3. J Biol Chem 278:18154–18161

Khan N, Gray IP, Obejero-Paz CA, Jones SW (2008) Permeation and gating in $Ca_V3.1$ (α1G) T-type calcium channels. Effects of Ca^{2+}, Ba^{2+}, Mg^{2+}, and Na^+. J Gen Physiol 132:223–238

Klemic KG, Shieh C–C, Kirsch GE, Jones SW (1998) Inactivation of Kv2.1 potassium channels. Biophys J 74:1779–1789

Klemic KG, Kirsch GE, Jones SW (2001) U-type inactivation of Kv3.1 and *Shaker* potassium channels. Biophys J 81:814–826

Kurata HT, Soon GS, Fedida D (2001) Altered state dependence of C-type inactivation in the long and short forms of human Kv1.5. J Gen Physiol 118:315–332

Kurata HT, Soon GS, Eldstrom JR, Lu GW, Steele DF, Fedida D (2002) Amino-terminal determinants of U-type inactivation of voltage-gated K^+ channels. J Biol Chem 277:29045–29053

Kurata HT, Doerksen K, Eldstrom JR, Rezazedeh S, Fedida D (2005) Separation of P/C- and U-type inactivation pathways in Kv1.5 potassium channels. J Physiol 14:14

Liu Y, Jurman ME, Yellen G (1996) Dynamic rearrangement of the outer mouth of a K^+ channel during gating. Neuron 16:859–867

López-Barneo J, Hoshi T, Heinemann SH, Aldrich RW (1993) Effects of external cations and mutations in the pore region on C-type inactivation of *Shaker* potassium channels. Recept Channels 1:61–71

MacKinnon R, Yellen G (1990) Mutations affecting TEA blockade and ion permeation in voltage-activated K^+ channels. Science 250(4978):276–279

Nguyen A, Kath JC, Hanson DC, Biggers MS, Canniff PC, Donovan CB, Mather RJ, Bruns MJ, Rauer H, Aiyar J, Lepple-Wienhues A, Gutman GA, Grissmer S, Cahalan MD, Chandy KG (1996) Novel nonpeptide agents potently block the C-type inactivated conformation of Kv1.3 and suppress T cell activation. Mol Pharmacol 50:1672–1679

Ogielska EM, Zagotta WN, Hoshi T, Heinemann SH, Haab J, Aldrich RW (1995) Cooperative subunit interactions in C-type inactivation of K channels. Biophys J 69:2449–2457

Rasmusson RL, Morales MJ, Castellino RC, Zhang Y, Campbell DL, Strauss HC (1995) C-type inactivation controls recovery in a fast inactivating cardiac K^+ channel (Kv1.4) expressed in *Xenopus* oocytes. J Physiol (Lond) 489:709–721

Smith PL, Baukrowitz T, Yellen G (1996) The inward rectification mechanism of the HERG cardiac potassium channel. Nature 379(6568):833–836